The C-terminal (haemopexin-like) domain structure of human gelatinase A (MMP2): structural implications for its function

Ulrich Gohlke[a,*,**], Franz-Xaver Gomis-Rüth[a], Thomas Crabbe[b], Gillian Murphy[c], Andrew J.P. Docherty[b], Wolfram Bode[a,*]

[a]*Max-Planck-Institut für Biochemie, Abteilung für Strukturforschung, Am Klopferspitz 18a, D-82152 Martinsried bei München, Germany*
[b]*Celltech Therapeutics, 216 Bath Road, Slough SL1 4EN, UK*
[c]*Strangeways Research Laboratory, Worts Causeway, Cambridge CB1 4RN, UK*

Received 28 November 1995

Abstract In common with most other matrix metalloproteinases, gelatinase A has a non-catalytic C-terminal domain that displays sequence homology to haemopexin. Crystals of this domain were used by molecular replacement to solve its molecular structure at 2.6 Å resolution, which was refined to an *R* value of 17.9%. This structure has a disc-like shape, with the chain folded into a β-propeller structure that has pseudo four-fold symmetry. Although the topology and the side-chain arrangement are very similar to the equivalent domain of fibroblast collagenase, significant differences in surface charge and contouring are observable on 1 side of the gelatinase A disc. This difference might be a factor in allowing the gelatinase A C-terminal domain to bind to natural inhibitor TIMP-2.

Key words: MMP; Gelatinase; Collagenase; Haemopexin; X-ray crystal structure

1. Introduction

The matrix metalloproteinases (MMPs) are a family of zinc-dependent endopeptidases that degrade components of the extracellular matrix [1]. Although required for normal development and maintenance, their activity has also been linked to the uncontrolled tissue destruction that accompanies many pathological conditions [2]. Gelatinase A (MMP2; EC 3.4.24.24, 72-kDa gelatinase, type-IV collagenase) is secreted by several cell types as the latent precursor, progelatinase A (proMMP2), and has recently been implicated in promoting tumour cell invasion [3], a role, which might be facilitated by its ability to bind to and be activated by constituents of the cell surface [4–8].

The primary sequence of the MMPs can be divided into functionally defined domains: the N-terminal propeptide lost upon activation, and the catalytic domain joined via a hinge region to a haemopexin-like C-terminal domain (CTD) possessed by all the MMPs except matrilysin (MMP7). The CTD of the collagenases (MMPs1 and 8) binds the enzymes to the collagens of types I–III [9,10], thereby positioning the substrate for cleavage at the active site [11]. MMP2 and the closely related gelatinase B (MMP9) also bind collagen but do so using 3 fibronectin-related type-II modules, which are inserted into their catalytic domains [12–16]. They efficiently degrade native type-IV and -V collagens, all denatured collagens, elastin, and fibronectin [12,13,17,18]; none of these activities is lost upon removal of the CTD [4] (G. Murphy, unpubl. results). The MMP2-CTD is required, however, for 3 particular properties of proMMP2: cell surface binding, activation [4–6], and binding of the proenzyme to the natural inhibitor TIMP-2 [5,19]. Indeed, the recent isolation of ternary complexes of proMMP2, TIMP-2, and MT-MMP (a membrane-bound MMP that activates proMMP2 [20]) suggests that the binding of TIMP-2 is of central importance to MMP2 function [21]. CTD interactions also assist in the inhibition of active MMP2 by TIMPs 1 and 2 [22].

In this report, the crystal structure of the MMP2-CTD is described. By comparing it to the recently obtained structure of the MMP-1 CTD [23], we make predictions concerning possible sites of interaction for TIMP-2.

2. Materials and methods

The active-site mutant Glu-375-Ala of human proMMP2 was overexpressed in mouse myeloma cells and isolated as previously described [19]. For crystallization, the sample was dialyzed in the absence of inhibitor against 4 mM MES, pH 7.5, 10 mM $CaCl_2$, 0.1 M NaCl, 0.02% w/v NaN_3. After adjusting the sample to 0.15 M citrate pH 6 and 2.5% PEG 6000 (Serva, Heidelberg, Germany), it was equilibrated against 0.9 M citrate at 20°C by hanging drop vapour diffusion. After about 2 months, small plate-shaped crystals appeared, which diffracted X-rays to 2.5 Å resolution. These crystals were of orthorhombic space group $P2_12_12_1$ and had the cell constants $a = 55.78$ Å, $b = 58.85$ Å and $c = 93.14$ Å. Examination of these crystals by SDS-PAGE and N-terminal sequencing revealed that the crystallized protein comprises the CTD of MMP2, extending from Ile-451 to Cys-660 (using the nomenclature of preMMP2 [12]).

X-ray intensity data were recorded on an imaging plate detector (MAR Research, Hamburg, Germany), using graphite monochromatized CuKα radiation. Data were processed using the MOSFLM v5.23 program package [24] and routines from the CCP4 suite [25]. The data collection statistics are summarized in Table 1.

The structure was solved by Patterson search methods using the coordinates of the CTD of full-length porcine MMP1 [23] kindly provided by Dr. P. Brick and colleagues as a search model. The search model comprised residues Cys-278 to Cys-466 of porcine MMP1 with all non-identical residues replaced by alanines. The rotational and translational search carried out with AMoRe [26] gave the highest solution with a correlation coefficient of 35.4 and an *R* factor of 56.2% ($C = 25.8$ and $R = 58.8\%$ for the second highest solution) in the resolution range 12.0–3.0 Å. A rigid-body refinement with AMoRe increased the correlation coefficient to 53.3 ($R = 51.8\%$).

All subsequent refinement steps were performed with X-PLOR [27]. The rigid-body refinement was repeated, allowing an independent

*Corresponding authors. Fax: (49) (89) 8578 3516.
E-mail: bode@biochem.mpg.de

***Present address:* EMBL, Meyerhofstrasse 1, D-69012, Heidelberg, Germany.

Abbreviations: MMP, matrix metallo proteinase; TIMP, tissue inhibitor of metalloproteinases; CTD, C-terminal domain.

SSDI 0014-5793(95)01435-7

movement of each of the 4 internal repeats of the CTD. After expansion of the resolution range to 12.0–2.6 Å and positional refinement, most of the new side-chains could unambigiously be built into the electron density map using the interactive graphics program FRODO [28]. Only at the amino acid insertion sites of MMP2-CTD, the electron density remained poorly defined. After several cycles of building and refinement against omit maps, a simulated annealing calculation was carried out [29], which improved the map. Two sodium ions, which were later replaced by calcium ions, a chloride and 78 water molecules were added. The B factors were refined individually, with restraints on bonded and angle-related atoms. The *R* factor of the final model is 17.9%, including data from 8 to 2.6 Å resolution; the rms deviations from standard values of bond length and angles [30] are 0.011 Å and 1.67°, respectively.

The first 7 residues of the protein, from Ile-451 to Pro-457, are fully disordered. The chain is defined by electron density from Thr-458 onwards. The main chain can be almost unambiguously traced down to the C-terminal Cys-660; only residues Thr-498 to Asp-501 are located in very weak density. Except for this site, only 2 peptide bonds, at Ile-468–Cys-469 and Ser-544–Ala-545, have bad difference densities; rebuilding leads to conformations with disallowed Ramachandran angles, however. The main chain angles of Asp-490 and Ala-545 are in 'generously allowed' regions. The program PROCHECK [31] incorporated in the CCP4 package indicates a favourable stereochemistry for all other non-Gly and non-Pro residues. Of the 17 Pro residues contained in the crystallized fragment, 2 (Pro-457 and Pro-499) are not properly defined, 3 (Pro-506, Pro-553 and Pro-603) are *cis*-prolines, while the remaining 12 have *trans*-conformation.

3. Results

Similar to the CTDs of porcine MMP2 [23] and of rabbit haemopexin [32], the CTD of MMP2 exhibits the shape of a flat cylindrical disc, with an approximate height and diameter of 25 and 40 Å, respectively. The polypeptide chain is essentially organized in 4 β-sheets I–IV, which are arranged almost symmetrically around a central axis giving rise to the formation of a 4-blade propeller (Fig. 1). Sheets I–IV are arranged in consecutive order around the central axis. Each sheet is made up of 4 antiparallel β-strands connected with a W-like strand topology. Each is strongly twisted, with the edge strands crossing over one another at an angle of about 60°.

The first, innermost strands in all 4 sheets enter the propeller at a common side (its 'entrance side') and run almost parallel to one another along the propeller axis forming a central tunnel, which opens slightly towards the other ('exit') side. Strands 1 and 2 are connected by short β-hairpin loops of 2 (sheet I)

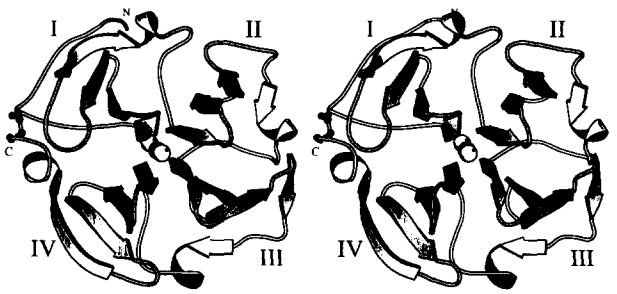

Fig. 1. Ribbon diagram (stereoview) of MMP2-CTD, shown against the exit side (see text). The domain is slightly tilted with respect to the pseudo four-fold symmetry axis of the β-propeller structure to clarify the tracing of the N-terminal extension peptide and the position of the ions in the central channel. The 4 propeller blades are numbered and the order of the ions is calcium (light grey), chloride (dark grey) and calcium (light grey). The disulphide bond is shown in CPK-fashion clamping the C-terminus to blade I (figure generated using the program MOLSCRIPT [35].)

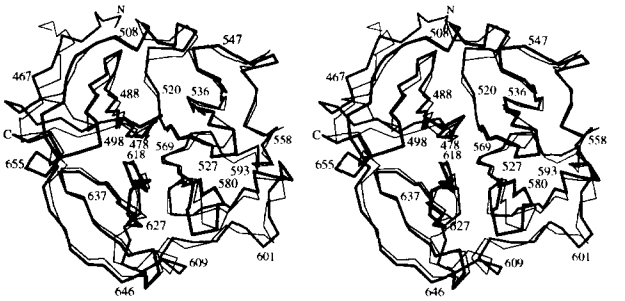

Fig. 2. Superposition (stereoview) of the Cα-chains of MMP2-CTD (thick line) and porcine MMP1 (thin line). The orientation of the domains is as in Fig. 1. The residues of MMP2-CTD are numbered at approximately 10-residue intervals (figure generated with MOLSCRIPT [35]).

to 4 residues (sheets II–IV), which are arranged around the more open exit of the tunnel, while the 1,4 tight turns connecting strands 2 and 3 form the entrance to the tunnel together with the entering segments. The 3→4 loop of blade A comprising 8 residues is quite open and partially flexible, whereas the corresponding loops in the other 3 blades are compact. The 4th strands of blades II and III are interrupted by characteristic β-bulges, which each are preceding a *cis*-Pro residue. The β-bulge and *cis*-Pro together form a structural insertion unit, which allows the accommodation of 3 extra residues in strand 4 (compared with sheet IV) without major sheet distortions (see Fig. 4). Both Pro residues are quite strongly conserved in the MMPs. Pro-506, likewise arranged in a *cis*-conformation, occupies an equivalent MMP2-CTD site in blade I. This Pro residue seems to be confined to both gelatinases, but is lacking in all other MMPs.

In all 4 blades, the outer strands loop around the periphery of the disc and end up in short 3_{10} (blades I and II) or α-helices (III and IV). The chain then turns towards the tunnel entrance to begin the first strand of the next blade. At the end of the α-helix terminating blade IV, the C-terminus is tethered to the entering strand of blade I via disulfide bridge 469–660. This clamping of the N and the C-terminus is obviously important for the integrity of the CTDs [10].

A quantitative comparison with the CTD of porcine MMP1 shows that the MMP2-CTD chain topology is quite similar and their secondary structure arrangement is virtually identical (Fig. 2). After optimal superposition of both domains, 171 Cα-atom pairs of topologically equivalent residues differ less than 3 Å, exhibiting an rms deviation of 1.22 Å. The corresponding sequence alignment based on this superposition is shown in Fig. 3. 66 topologically equivalent residues out of the 192 residues contained in MMP2-CTD, i.e. 35%, turn out to be identical. In general, the 4 sheets superimpose well, with only a slight increase in deviation towards the periphery (see Fig. 2). Larger deviations are only found in some of the β-hairpin loops. Most noteworthy is the differing chain course in the large 3→4 loop of blade I, where the MMP2-CTD chain is partially undefined. Smaller, but significant deviations occur in the 1→2 loops of blades II–IV (two residue insertion in MMP2), and in the 3→4 loop of blade III. All of these differing loops are located on the exit side of the disc.

The internal (pseudo) four-fold symmetry of the haemopexin-like domain is reflected to a high degree in the

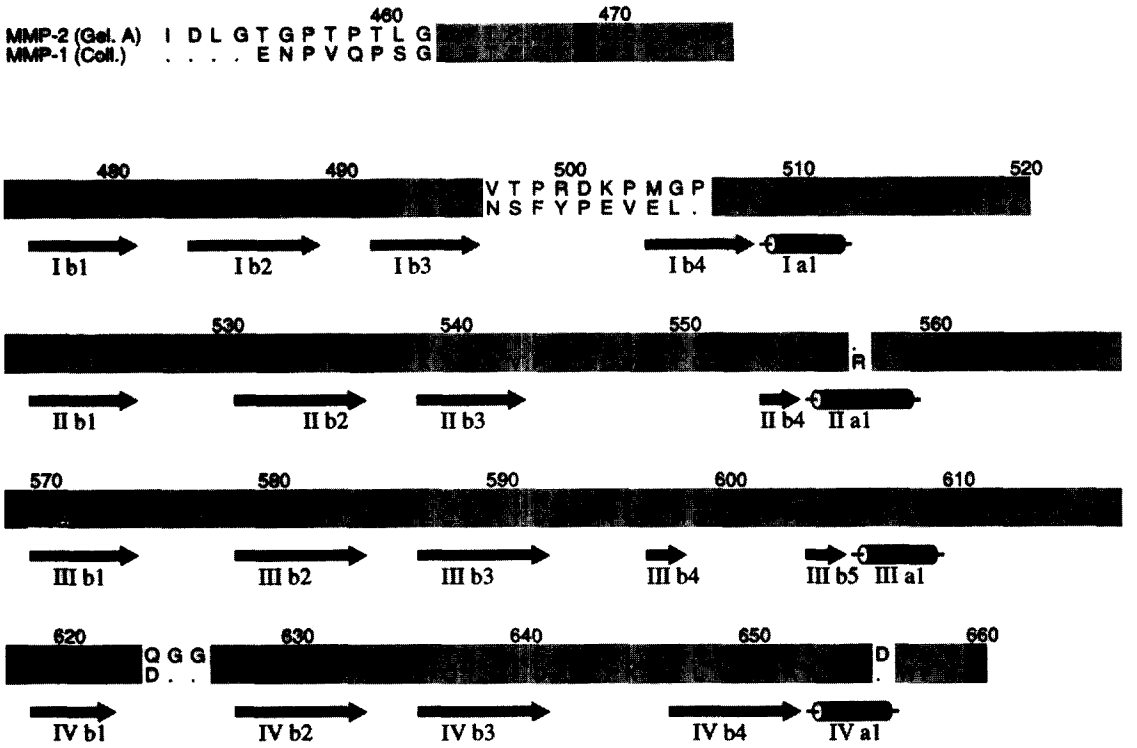

Fig. 3. Amino acid sequence alignment of MMP2-CTD and porcine MMP1. Sequence data were taken from the PIR database. Alignment is based on comparison of the spatial structures (this work, [23]). The N-terminal extension as well as the 4 domains of the β-propeller structure are shown, with the secondary structure elements indicated for MMP2-CTD according to the definition of Kabsch and Sander [37]. Arrows represent β-strands, cylinders α-helices. Structurally equivalent regions are shaded (light grey). The cysteines of the disulphide bond as well as the Ca^{2+}-binding aspartates are boxed in dark grey (figure generated using the program ALSCRIPT [38]).

similar scaffold architecture of the 4 blades (Fig. 4). This similarity is particularly strong between blades II–IV, where the Cα-atoms of the approximately 30 residues involved in β-sheet formation exhibit rms deviations of 0.8–0.95 Å. Blade I differs most, mainly due to its larger 3→4 loop and its more deviating 4th strand. Alignment of the 4 chain segments forming blades I–IV, done according to the topological equivalence, shows a 15–30% identity within the sheet segments, again with blade I ranking lowest; the degree of residue similarity is considerably larger, however (see Fig. 3).

The CTD disc is evenly filled with protein atoms, in spite of its volume, which has a strong radial increase. This is mainly achieved by an increase in the size of the contributing amino acids when going from the centre to the periphery. The internal strands are characterized by a preponderance of Ala residues, while strands 2 and 3 preferentially harbour large mainly aromatic residues, such as Phe and Trp. The hydrophobic side-chains projecting from each sheet in an alternating manner combine with the corresponding side-chains of adjacent blades to form large hydrophobic clusters at the blade interfaces. Many of the contributing (aromatic) residues are identical or similar between the CTDs of MMP2 and porcine MMP1, and most of them are highly conserved in all MMPs. Towards the radial periphery, these hydrophobic regions are largely covered by the connecting helical fragments, which are anchored in these clusters via hydrophobic side-chains. Towards the exit side, these hydrophobic clusters are partially exposed to the bulk solvent.

A prominent feature of the MMP2-CTD is the tunnel traversing the centre of the disc (see Fig. 1). It is formed by the 4 inner strands, which run parallel and are arranged in register. Due to a slight curvature in these strands, this tunnel opens

Table 1
Statistics for data collection and refinement

Data collection	
Dataset	NATI
Maximal resolution	2.6 Å
Reflections measured	34708
Unique reflections ($I > 4\sigma(I)$)	9618
Rmerge[a]	0.069 (∞–2.60 Å)
	0.274 (2.65–2.60 Å)
Completeness	96.7% (∞–2.60 Å)
	71.3% (2.65–2.60 Å)
Refinement	
Resolution	8.0–2.6 Å
Reflections	8574
R factor[b]	17.9%
Total number of non-hydrogen atoms	1645
Number of active non-hydrogen atoms	1603
Number of waters	73
Ions	3
Geometry rms deviations	
Bond distances	0.011 Å
Angles	1.67°
Mean B factor	19.1 Å^2

[a] Rmerge = $\Sigma_h\Sigma_i|I(h,i)-\langle I(h)\rangle|/\Sigma_h\Sigma_i I(h,i)$.
[b] R factor = $(\Sigma||Fo|-|Fc||)/\Sigma|Fo| \times 100$.

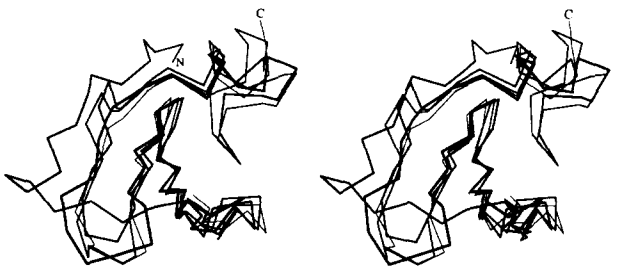

Fig. 4. Superposition of the Cα-chains of the 4 blades of MMP2-CTD (stereoview). Orientation is as of blade I in Fig. 1. The range of each blade is taken as in the sequence alignment (Fig. 3). The 4 blades are drawn with decreasing line thickness, with blade I having the thickest and blade IV the thinnest line (superposition was calculated with LSQMAN [36]; figure generated with MOLSCRIPT [35]).

somewhat towards the exit side. Within this tunnel, 4 ions/solvent molecules are found arranged along the pseudo four-fold axis, which tentatively have been assigned as 2 Ca^{2+} ions, a Cl^- ion and a water molecule (Fig. 5), based on their scattering power and coordination geometry. The crystallization and the harvesting buffer contained high amounts of Ca^{2+} and Cl^-, besides Na^+ and citrate. The first of the Ca^{2+} ions, KA5, is positioned at the entrance to the tunnel, where it is tetragonally surrounded by the first carbonyl groups of each inner strand, donated by Asp-476, Asp-521, Asp-569 and Asp-618. The Ca^{2+}–oxygen distances are 2.4–2.5 Å, i.e. only slightly exceed mean values of Ca^{2+}–carbonyl interactions in protein structures (2.36 Å [33]). The B value of this Ca^{2+} refines to 15 Å^2, comparable to that of the coordinating carbonyl oxygens. A water molecule (W28), localized just outside of the tunnel entrance at a distance of 2.9 Å, slightly away from the tunnel axis, forms the 5th Ca^{2+} ligand and occupies the vertex of a distorted tetragonal pyramid. Such a Ca^{2+} coordination by only 5 oxygen ligands is not frequently observed, but might be forced here by the special tunnel environment. It is noteworthy that the side-chains of the 4 Asp residues contributing the carbonyl ligands are neither direct Ca^{2+} ligands nor connected to it via the localized water ligand, due to structural restraints imposed from the main chain. An equivalent calcium ion with identical binding geometry has been observed in the porcine MMP1 structure [23] and in the haemopexin domain [32].

The centre of the tunnel harbours an anion–cation couple (Fig. 5), which has been modeled as a Cl^-–Ca^{2+} pair (a Na^+ such as assumed in the haemopexin structure [32] would have unusually low B values). The Ca^{2+} (KA2, B = 20 Å^2) is octahedrally surrounded by 6 ligands, with the 4 carbonyl oxygens of Ile-478, Val-533, Ala-571 and Val-620 placed at the corners of the central tetragonal plane. The Cl^- ion and a solvent molecule (W33) occupy the vertices in the tunnel centre and its exit, respectively (Fig. 5). The distances from the central Ca^{2+} ion to the 4 carbonyl oxygens are 2.6–2.7 Å, while 2.4 and 3.1 Å to the water and the Cl^-, respectively. Another more distant water molecule is positioned towards the tunnel exit, but away from its axis. The Cl^- ion (B = 31 Å^2) is tetragonally surrounded by the amide nitrogens of the same 4 residues, which also provide the KA2 carbonyl ligands. In agreement with the relatively large ionic radius of Cl^- (1.94 Å [34]), the Cl^-–nitrogen distances are 3.8–4.0 Å. In the porcine MMP1 structure, 2 spheres of isolate density in the centre of the tunnel were interpreted as water molecules, however, with quite unusual ligand interactions. In the haemopexin structure, a similar electron density was believed to account for a Cl^-–Na^+ couple, with an additional phosphate anion bound to the sodium.

The overall number of positively (26) and negatively charged residues (25) in MMP2-CTD is almost equal, their distribution over the molecular surface is, however, not uniform. In general, the acidic residues are preferentially clustered at both flat sides of the disc-like molecule, whereas the basic residues are predominantly found at the radial periphery. In particular the entry side is characterized by a negative electrostatic potential. Most of all, the 4 uncompensated Asp residues arranged around the tunnel entrance contribute to this potential and could provide strong anchoring points for approaching ligands of opposite charge. On the exit side, a surface patch of positively charged residues centered around Lys-595, Lys-596 and Lys-597 is noteworthy, and extends from the tunnel exit along the surface of blade III towards the periphery. Most of the underlying basic residues are also found in other MMPs. Only Lys-597 and Arg-550, the latter situated on the exposing β-bulge of blade II, are truly specific to MMP2.

The initial (structurally defined) part of the linker peptide projects 5 residues in the axial direction out of the periphery of blade I (see Fig. 1). It exhibits an almost extended conformation, which is supported only by a few weak intermolecular contacts with a symmetry-related molecule. From Pro-463 to Cys-469, this linker is in direct contact with the own CTD nestling against the 4th strand of blade I. A comparison with the full-length chain of the porcine MMP1 molecule (Fig. 2) shows that the course of this linker is quite similar from Pro-463 onwards. Due to a slight kink at this Pro residue, the preceding fragments deviate slightly from one another, with both fragments exhibiting extended conformations.

4. Discussion

Structural analysis of the MMP2-CTD reveals that it is topologically quite similar to that of porcine MMP1. The only significant conformational differences occur at the exit side of the disc, although both entry and exit sides display different charge patterns. The overall similarity is in agreement with the

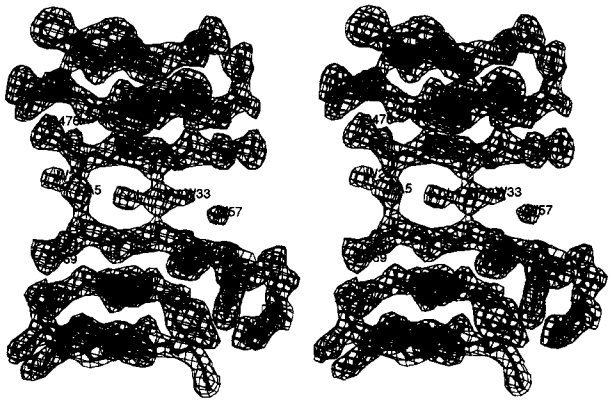

Fig. 5. Section through the refined MMP2-CTD structure along the tunnel axis, superimposed with the final electron density contoured at 1 σ (stereoview). Shown are the first 3 strands of blades I and III, respectively, together with the ions and solvent molecules arranged along the tunnel axis (figure generated with FRODO [28].

close sequence homology that exists between these 2 MMPs (Fig. 3), and might be enforced by the many constraints that exist in this β-propeller structure.

The CTD of porcine MMP1 is connected to the catalytic domain by a short bulged segment and an extended linker peptide [23], which our structure suggests is a general feature of the MMPs. It is proposed that the MMP1 linker peptide acts as a fitting spacer that allows the entry side of the CTD to fold over the catalytic domain, thereby trapping bound triple helical collagen substrate at the active site cleft [11].

MMP2 does not use the CTD to bind collagen [15], but its linker peptide may instead be involved in correctly positioning bound TIMP-2. This is of importance to the inhibition of the active enzyme, because the interaction of the CTDs of TIMP-2 and MMP2 allows the N-terminal domain of TIMP-2 efficiently to dock with the enzyme's active site [22]. Sequence comparison of the TIMPs revealed that TIMP-2 possesses a negatively charged 'tail'. Removal of this tail decreased the association rate constant of TIMP-2 and active MMP2 and prevented the inhibitor from binding to proMMP2 [22]. It is possible, therefore, that the positively charged region located on the exit side and the periphery of blade III of the MMP2-CTD represents an anchoring site for TIMP-2. This is speculative and must be tested by generating mutants, in which the internal structure is unaltered. The MMP2-CTD structure described in this report provides a good foundation for the design of such experiments.

Acknowledgements: We thank Professor R. Huber for his constant encouragement, Dr. T. Mather for careful reading, Dr. J. Kellermann for sequencing and Dr. P. Brick for making the coordinates of porcine MMP2 available to us. The financial support of the SFB207 of the University of Munich (W.B.) and by the EEC program 'Human Capital and Mobility', Contract CHRX-CT94-0535 (W.B. and F.-X. G.-R.) is kindly acknowledged.

References

[1] Birkedal-Hansen, H., Moore, W.G.I., Bodden, M.K., Windsor, L.J., Birkedal-Hansen, B., DeCarlo, A. and Engler, J.A. (1993) Crit. Rev. Oral Biol. Med. 4, 197–25O.
[2] Woessner, J.F., Jr. (1991) FASEB J. 5, 2145–2154.
[3] Stetler-Stevenson, W.G., Aznavoorian, S. and Liotta, L.A. (1993) Annu. Rev. Cell. Biol. 9, 541–573.
[4] Murphy, G., Willenbrock, F., Ward, R.V., Cockett, M.I., Eaton, D. and Docherty, A.J.P. (1992) Biochem. J. 283, 637–641.
[5] Strongin, A.Y., Marmer, B.L., Grant, G.A. and Goldberg, G.I. (1993) J. Biol. Chem. 268, 14033–14039.
[6] Ward, R.V., Atkinson, S.J., Reynolds, J.J. and Murphy, G. (1994) Biochem. J. 304, 263–269.
[7] Emmert-Buck, M.R., Emonard, H.P., Cocoran, M.L., Krutzsch, H.C., Foidart, J.-M. and Stetler-Stevenson, W.G. (1995) FEBS Lett. 364, 28–32.
[8] Chen, W.-T. (1992) Curr. Opin. Cell Biol. 4, 8O2–8O9.
[9] Murphy, G., Allan, J.A., Willenbrock, F., Cockett, M.I., O'Connell, J.P. and Docherty, A.J.P. (1992) J. Biol. Chem. 267, 9612–9618.
[10] Hirose, T., Patterson, C., Pourmotabbed, T., Mainadi, C.L. and Hasty, K.A. (1993) Proc. Natl. Acad. Sci. USA 90, 2569–2573.
[11] Bode, W. (1995) Structure 3, 527–531.
[12] Collier, I.E., Wilhelm, S.M., Eisen, A.Z., Marmer, B.L., Grant, G.A., Seltzer, J.L., Kronberger, A., He, C., Bauer, E.A. and Goldberg, G.I. (1988) J. Biol. Chem. 263, 6579–6587.
[13] Wilhelm, S.M., Collier, I.E., Marmer, B.L., Eisen, A.Z., Grant, G.A. and Goldberg, G.I. (1989) J. Biol. Chem. 264, J7213–17221.
[14] Collier, I.E., Krasnov, P.A., Strongin, A.Y., Birkedal-Hansen, H. and Goldberg, G.I. (1992) J. Biol. Chem. 267, 6i76–6781.
[15] Murphy, G., Nguyen, Q., Cockett, M.I., Atkinson, S.J., Allan, J.A., Knight, C.U., Willenbrock, F. and Docherty, A.J.P. (1994) J. Biol. Chem. 269, 6632–6636.
[16] Steffensen, B., Wallon, U.M. and Overall, C.M. (1995) J. Biol. Chem. 270, 11555–11566.
[17] Murphy, G., Cockett, M.I., Ward, R.V. and Docherty, A.J.P. (1991) Biochem. J. 277, 277–279.
[18] Fukai, F., Ohtaki, M., Fujii, N., Yajima, H., Ishii, T., Nishizawa, Y., Miyazaki, K. and Katayama, T. (1995) Biochernisrry 34, 11453–11459.
[19] Crabbe, T., Zucker, S., Cockett, M.I., Willenbrock, F., Tickle, S., O'Connell, J.P., Scothern, J.M., Murphy, G. and Docherty, A.J.P. (1994) Biochemistry 33, 6684–6690.
[20] Sato, H., Takino, T., Okada, Y., Cao, J., Shinagawa, A., Yamamoto, E. and Seiki, M. (1994) Nature (London) 370, 61–65.
[21] Strongin, A.Y., Collier, I.E., Bannikov, U., Marner, B.L., Grant, G.A. and Goldberg, G.I. (1995) J. Biol. Chem. 270, 5331–5338.
[22] Willenbrock, F., Crabbe, T., Slocombe, P.M., Sutton C., Docherty, A.J.P., Cockett, M.-I., O'Shea, M., Brocklehurst, K., Phillips, I.R. and Murphy, G. (1993) Biochemistry 32, 4330–4337.
[23] Li, J., Brick, P., O'Hare, M.C., Skarzynski, T., Lloyd, L.F., Curry, V.A., Clark, I.M., Bigg, H.F., Hazleman, B.L., Cawston, T.E. and Blow, D.M. (1995) Structure 3, 541–549.
[24] Leslie, A.G.W. (1991) in Crystallographic Computing V. (Moras, D., Podjarny, A.D. and Thierry, J.C., Eds.), pp. 27–38, Oxford University Press, Oxford, UK.
[25] Collaborative Computational Project, Number 4 (1994) Acta Crystallogr. D 50, 760–763.
[26] Navaza, J. (1994) Acta Crystallogr. A 50, 157–163.
[27] Brünger, A.T. (1992) X-Plor Version 3.1. A System for X-Ray Crystallography and NMR. Yale University Press, New Haven, CT.
[28] Jones, T.A. (1978) J. Appl. Cryst. 15, 23–31.
[29] Brünger, A.T. (1991) Annu. Rev. Phys. Chem. 42, 197–223.
[30] Engh, R.A. and Huber, R. (1991) Acta Crystallogr. A 47, 392–400.
[31] Laskowski, R.A., MacArthur, M.W., Moss, D.S. and Thornton, J.M. (1993) J. Appl. Cryst. 26, 283–291.
[32] Faber, H.R., Groom, C.R., Baker, H.M., Morgan, W.T., Smith, A. and Baker, E.N. (1995) Structure 3, 551–559.
[33] McPhalen, C.A., Strynadka, N.C.J. and James, M.N.J. (1991) Adv. Prot. Chem. 42, 77–144.
[34] Pauling, L. (1948) in The Nature of the Chemical Bond. Cornell University Press, Ithaca, NY.
[35] Kraulis, P.J. (1991) J. Appl. Cryst. 24, 946–950.
[36] Kleywegt, G.J. and Jones, T.A. (1994) in From First Map to Final Model (Bailey, S., Hubbard, R. and Waller, D., Eds.), SERC, Daresbury Laboratory, pp. 59–66.
[37] Kabsch, W. and Sander, C. (1983) Biopolymers 22, 2577–2637.
[38] Barton, G.J. (1993) Protein Eng. 6, 37–40.

Note added in proof.

Meanwhile we have become aware of a paper of Libson et al. (1995) Nature Struct. Biol. 2, 938–941, describing the same molecule in a slightly different crystal form.